



OPEN

## Minimal system for assembly of SARS-CoV-2 virus like particles

Heather Swann<sup>1,2,5</sup>, Abhimanyu Sharma<sup>2,5</sup>, Benjamin Preece<sup>1,2</sup>, Abby Peterson<sup>1,2</sup>, Crystal Eldridge<sup>1,2</sup>, David M. Belnap<sup>3,4</sup>, Michael Vershinin<sup>1,2,3</sup>✉ & Saveez Saffarian<sup>1,2,3</sup>✉

SARS-CoV-2 virus is the causative agent of COVID-19. Here we demonstrate that non-infectious SARS-CoV-2 virus like particles (VLPs) can be assembled by co-expressing the viral proteins S, M and E in mammalian cells. The assembled SARS-CoV-2 VLPs possess S protein spikes on particle exterior, making them ideal for vaccine development. The particles range in shape from spherical to elongated with a characteristic size of  $129 \pm 32$  nm. We further show that SARS-CoV-2 VLPs dried in ambient conditions can retain their structural integrity upon repeated scans with Atomic Force Microscopy up to a peak force of 1 nN.

### Main

COVID-19 is a pandemic disease caused by infection of SARS-CoV-2 virus<sup>1</sup>. With more than 5 million cases confirmed and a death toll exceeding several hundred thousand individuals, a search for antiviral therapies as well as vaccine candidates is of utmost urgency. Non-infectious virus like particles (VLPs) displaying essential viral proteins can be used to study the structural properties of the SARS-CoV-2 virions and due to their maximum immunogenicity are also vaccine candidates<sup>2,3</sup>. VLPs are released from cells with similar mechanisms as fully infectious virions and resemble the shape and composition of fully infectious virions<sup>4</sup>. Most Coronaviruses are pathogens of zoonotic nature with different viruses infecting avian (IBV), bovine (BCoV), porcine (TGEV), feline (FIPV) and murine(MHV) species<sup>4</sup>. There is evidence that Bat-SARS-CoV is the origin of the SARS-CoV virus which first appeared in human hosts in 2003<sup>5</sup>. The genome of SARS- CoV-2 has ~ 90% similarity to genome of coronaviruses previously identified in bat populations in China<sup>1,6</sup>.

VLPs with similar sizes to wild type TGEV are released by expression of E and M proteins of TGEV<sup>7</sup>. Similar results are reported for IBV<sup>8</sup>. Similarly, expression of M, E and S proteins are shown to result in release of morphologically identical particles to wild type SARS-CoV virus<sup>9,10</sup>. It is known that TGEV VLPs can induce an IFN $\alpha$  response in their hosts<sup>7</sup>. More recently human MERS-CoV VLPs were also shown to elicit an immune response and serve as vaccine candidates<sup>11</sup>.

Given the similarities between SARS-CoV-2 and SARS-CoV viruses<sup>1,12</sup>, we set out to create SARS-CoV-2 VLPs by expressing S, M and E proteins of SARS-CoV-2 in mammalian cells. Since SARS-CoV-2 virions have been reported to survive on solid surfaces in dry conditions for many hours<sup>13</sup>, we tested the structural integrity of the SARS- CoV-2 VLPs attached to dry glass using Atomic Force Microscopy (AFM).

### Methods

**Plasmid preparation and VLP harvest.** SARS-CoV-2 M, S and E protein genes were identified from the full genome sequence of the virus<sup>1</sup>, these genes were then humanized and inserted in CMV driven mammalian expression vectors (see supplement for complete plasmid sequences). 24 h after transfecting a monolayer of 293 T cells with a cocktail of S, M and E plasmids, VLPs were harvested from the supernatant (see supplement for further details). The supernatant was filtered using 0.2um filter and VLPs were captured in a 40–10% sucrose step gradient and concentrated using AMICON spin filters (UFC901008, EMD Millipore, Burlington, MA). Total protein yield for purified VLP stock varied somewhat but was typically above 5 mg/mL. The purified VLPs were stable for at least a week when stored at ~ 4 °C.

**Immunogold electron microscopy.** VLPs were incubated with 1:1000 dilution of anti-S antibody (clone 1A9, GTX632604, GeneTex, Irvine, CA) and 1:5 dilution of goat anti-mouse IgG nanogold conjugates (BBI solutions, Crumlin, UK, distributed by TedPella, Redding, CA, cat # 15,753). Negative stain electron microscopy

<sup>1</sup>Center for Cell and Genome Science, University of Utah, Salt Lake City, USA. <sup>2</sup>Department of Physics and Astronomy, University of Utah, Salt Lake City, USA. <sup>3</sup>School of Biological Sciences, University of Utah, Salt Lake City, USA. <sup>4</sup>Department of Biochemistry, University of Utah, Salt Lake City, USA. <sup>5</sup>These authors contributed equally: Heather Swann and Abhimanyu Sharma. ✉email: Vershinin@Physics.utah.edu; Saffarian@Physics.utah.edu

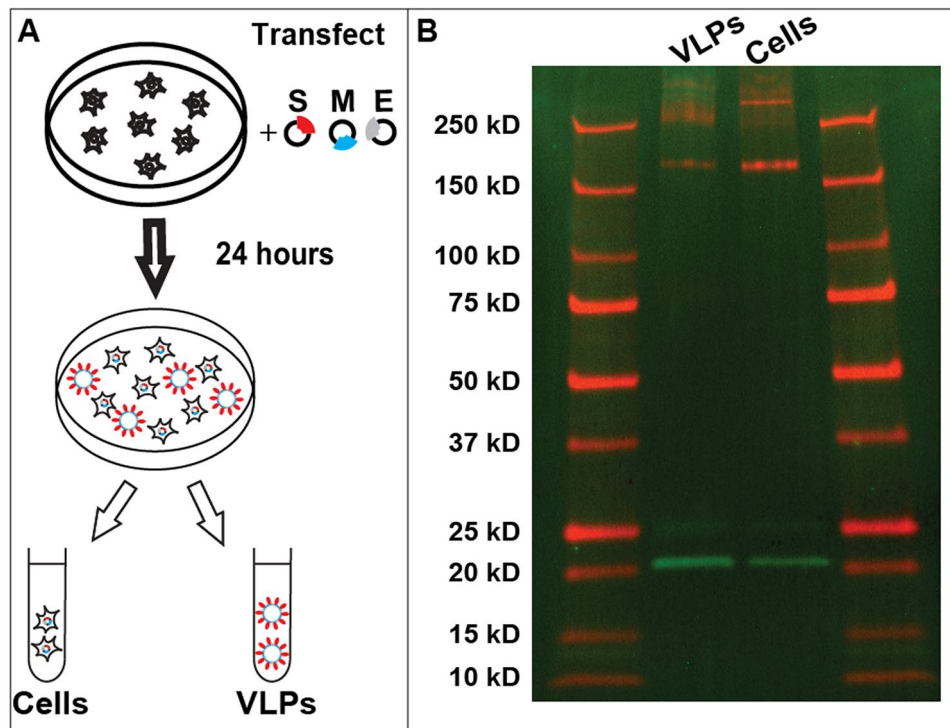


**Figure 1.** VLP expression and characterization using western blots. **(A)** Schematic representation of transfection and VLP harvest. **(B)** Western blot analysis of cells as well as VLPs separated as explained in methods. The gel was performed simultaneously, scanned at 700 nm and 800 nm, then superimposed using ImageJ (NIH) color merge for greater clarity, followed by cropping and minimal contrast enhancement. S protein (red) and M protein (green) are seen in two middle lanes. S protein tends to aggregate at very high concentrations (Fig. S2) resulting in smeared signal above 250 kD. S protein cleavage product is seen at 75 kD however the band is better visible when imaging channels are shown separately (Fig. S6). Protein size standards are described in “Methods” and are seen in leftmost and rightmost lanes. All size standard bands are also annotated on the left.

was performed on VLPs by applying 3.5  $\mu$ L of VLPs to a glow-discharged formvar-carbon coated EM grid (Ted Pella, Redding, CA) followed by two de-ionized water washes and staining with 1% uranyl acetate. Imaging was performed in a JOEL JEM1400-Plus microscope with an accelerating voltage of 120 keV.

**Western Blot analysis.** After triple washing the cells with PBS, 293 T cells were suspended in 100ul of RIPA buffer (sc-24948, Santa Cruz, Dallas, Texas). 10  $\mu$ L of VLPs or cell extracts were then denatured by Laemmli sample buffer (BioRad, Hercules, CA) with 5% BME and boiled at 95C for 10 min. The proteins were separated by SDS-PAGE and then transferred to a PVDF membrane (Millipore, Burlington, Massachusetts). Membranes were stained with 1:1000 dilution of Anti-SARS-CoV S $\Delta$ 10 antibody ([1A9], GenTex, Irvine, CA) along with 1:1000 dilution of Anti-Membrane Protein (2019-nCoV) Polyclonal Antibody (NCV-M-005, eEnzyme, Gaithersburg, MD) and then immunoprobed with appropriate infrared secondary antibody. Both antibodies were confirmed to be specific to intended antigens (Fig. S3) Membrane was scanned with the Odyssey infrared imaging system (LI-COR, Lincoln, NE) according to the manufacturer’s manual instruction at 700 nm and 800 nm.

**AFM sample prep and experiments.** AFM experiments were performed using Dimension Icon AFM with an MLCT-BIO-DC probe (Bruker, Santa Barbara, CA, USA) in PeakForce QNM in air mode at room temperature. Glass coverslips were functionalized with anti-S antibody as follows. Glass was first cleaned and functionalized with biotin-PEG-silane as previously described<sup>15</sup>. The surfaces were then incubated with neutravidin (Thermo Scientific Pierce Protein Biology, Waltham, MA, USA) followed by a brief dd-H<sub>2</sub>O wash to get rid of excess neutravidin and incubation with biotinylated anti-S antibody (11-2001-B, Abcam, San Diego, CA, USA). Surfaces thus prepared were generally devoid of debris but sometimes had step-edge character suggesting that antibody coating was less than a full monolayer (Fig. S4). The VLPs suspended in assay buffer were then incubated with the functionalized surface and finally washed away via brief buffer exchange with dd-H<sub>2</sub>O followed by drying under Nitrogen gas flow. All incubations lasted 30 min at room temperature. Assay buffer: PBS, pH 7.

## Results

VLP purifications were first assessed biochemically. Figure 1 (see also Fig. S1) shows western blot analysis of cell extracts as well as purified VLPs. The isolated VLPs have both M and S proteins as identified in western blots. S protein appears more highly enriched in cells vs VLPs suggesting that not all expressed S protein is released on VLPs. The isolated VLPs were further analyzed by running a 10–40% sucrose gradient and sequential

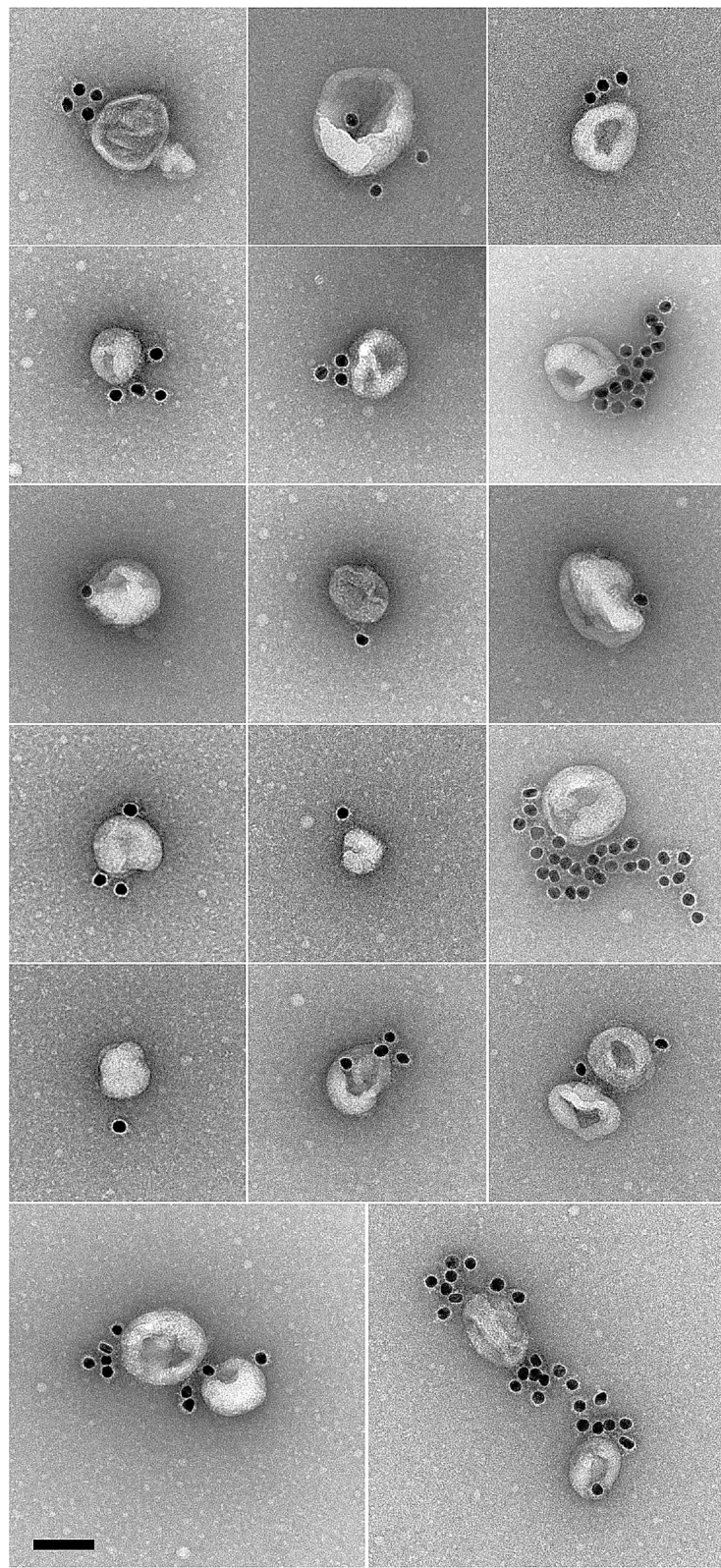


**Figure 2.** Negative stain electron microscopy reveals SARS-CoV-2 VLPs specifically labeled with immunogold. Scale bar : 100 nm.

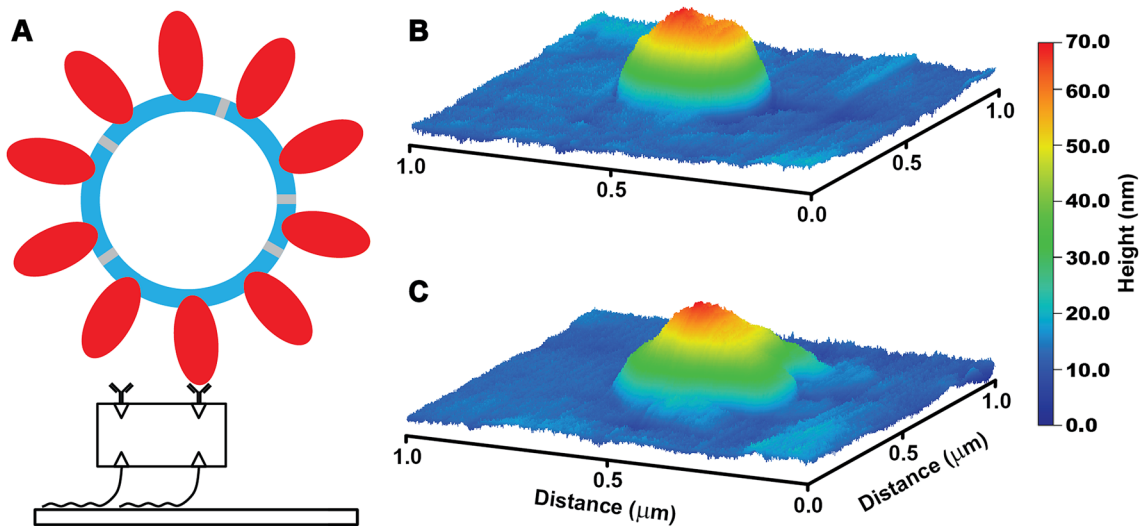


**Figure 3.** VLP surface immobilization and imaging. (A) Schematic of VLP-surface attachment strategy (bottom to top): glass surfaces were functionalized with Biotin-PEG-Silane, then neutravidin, then biotinylated anti-S antibody which then allowed for the capture of purified VLPs. VLP imaging showed initially symmetric particles. (B) which developed prominent deformations likely indicative of bursts upon repeated AFM imaging with 1 nN peak force (C).

fractionation. VLPs were found to be within the density of 20–25% sucrose (Fig. S2). S protein bands show a cleavage product which runs at a lower molecular weight from full S protein as shown in Fig. 1 and more clearly visible in Fig. S2. In addition both S protein as well as M protein form complexes which survive during western blot analysis and run at considerably higher molecular weight; successive dilutions results in breakup of these higher molecular weight fractions to respective monomeric bands for each protein (Fig. S3).

We further characterized the purified VLPs via electron microscopy. Figure 2 shows a representative image of the electron micrographs with the immobilized VLPs on the EM grids. VLPs can be identified via specific nanogold immunolabeling. Notably, nanogold labels not only decorate the VLPs but also proximal areas, suggestive of S protein dissociating from VLPs during surface deposition. The SARS-CoV-2 VLPs we have characterized have a size distribution of  $129 \pm 32$  nm, consistent with the general characterization of prior coronaviruses with size distributions of 100–200 nm<sup>4</sup>. This is also consistent with prior reports for SARS-CoV VLPs, which were characterized with crytomography and have size distribution of 79–224 nm (shape reportedly varied from nearly spherical to ellipsoidal with a 2 to 1 aspect ratio<sup>9</sup>). Our measured VLPs are also consistent with limited electron microscopy data available for the fully infectious SARS-CoV-2 virions observed in patient samples<sup>14</sup>.

The structural integrity of VLPs can inform their practical applications as well as serve as an estimate of the stability of fully infectious SARS-CoV-2 virions. We therefore further characterized the VLPs on functionalized surfaces with atomic force microscopy (AFM) (Fig. 3 and Figs. S5 & S6). VLPs were independently imaged on multiple occasions, originating from multiple purification batches. The observed surface density was as high as  $\sim 100$  per  $10 \mu\text{m}$  square field of view for high-yield VLP batches. VLPs appeared as approximately spherically symmetric particles whose lateral diameter was in excess of 200 nm while heights of the particles varied between 50 and 60 nm. These shapes are consistent with VLP dimensions broadened laterally by imaging forces and tip curvature and reduced somewhat in height due to surface adhesion and possibly imaging forces. Although detailed characterization is subject of future work, we found that repeated imaging of VLPs with peak force of 1 nN led to gradual particle deformations: reduced particle heights and non-circular lateral cross-sections – consistent with VLP bursts (Fig. 3C and Fig. S6). This force is within the range of previously reported values (0.5–5 nN) for bursting various virus capsids<sup>15,16</sup> although most prior work has been done in liquid. Our observations represent an upper estimate of the rupture force for SARS-CoV-2. This demonstrates that SARS-CoV-2 VLPs can be disrupted by direct application of moderate mechanical perturbations and open the door for future studies of VLP mechanics and integrity.

## Discussion

Expression of just M, S, and E proteins (Fig. 1) was sufficient for release of VLPs which were structurally competent for both harvesting and subsequent investigations (Figs. 2, 3). These results open the door for many further studies. They can serve as immunogenic agents in place of the full infectious virus. The VLPs can also serve to study virus interactions with proteins of interest (e.g. receptors)—to date most such studies were only possible at the single protein level or in the context of the infectious virus. In addition, artificial VLPs can now be used to study the mechanical properties of the SARS-CoV-2 virus as well as their dependence on environmental conditions. Finally, VLPs can also be used to develop and validate novel testing strategies for SARS-CoV-2. The expression methodology is robust and should require no modifications to create VLPs for most S, M, and E mutations found in native conditions<sup>17</sup>.

## Data availability

For expediency, genetic material in this work is published in the supplement and is available from the authors upon request. The authors will deposit the genetic material with Addgene.

Received: 29 May 2020; Accepted: 26 November 2020

Published online: 14 December 2020

## References

1. Wu, F. *et al.* A new coronavirus associated with human respiratory disease in China. *Nature* **579**, 265–269 (2020).
2. Prompetchara, E., Ketloy, C. & Palaga, T. Immune responses in COVID-19 and potential vaccines: Lessons learned from SARS and MERS epidemic. *Asian Pac. J. Allergy Immunol.* **38**, 1–9 (2020).
3. Zumla, A., Chan, J. F. W., Azhar, E. I., Hui, D. S. C. & Yuen, K.-Y. Coronaviruses—drug discovery and therapeutic options. *Nat. Rev. Drug Discov.* **15**, 327–347 (2016).
4. Masters, P. S. In *Advances in Virus Research* Vol. 66, 193–292 (Academic Press, 2006).
5. Lau, S. K. P. *et al.* Severe acute respiratory syndrome coronavirus-like virus in Chinese horseshoe bats. *Proc. Natl. Acad. Sci. U. S. A.* **102**, 14040–14045 (2005).
6. Hu, D. *et al.* Genomic characterization and infectivity of a novel SARS-like coronavirus in Chinese bats. *Emerg. Microbes Infect.* **7**, 154–154 (2018).
7. Baudoux, P., Carrat, C., Besnard, L., Charley, B. & Laude, H. Coronavirus pseudoparticles formed with recombinant M and E proteins induce alpha interferon synthesis by leukocytes. *J. Virol.* **72**, 8636–8643 (1998).
8. Corse, E. & Machamer, C. E. Infectious bronchitis virus E protein is targeted to the Golgi complex and directs release of virus-like particles. *J. Virol.* **74**, 4319–4326 (2000).
9. Neuman, B. W. *et al.* A structural analysis of M protein in coronavirus assembly and morphology. *J. Struct. Biol.* **174**, 11–22 (2011).
10. Mortola, E. & Roy, P. Efficient assembly and release of SARS coronavirus-like particles by a heterologous expression system. *FEBS Lett.* **576**, 174–178 (2004).
11. Wang, C. *et al.* MERS-CoV virus-like particles produced in insect cells induce specific humoral and cellular immunity in rhesus macaques. *Oncotarget* **8**, 12686–12694 (2017).
12. Marra, M. A. *et al.* The genome sequence of the SARS-associated coronavirus. *Science* **300**, 1399–1404 (2003).
13. Chin, A. W. H. *et al.* Stability of SARS-CoV-2 in different environmental conditions. *Lancet Microbe* **1**, e10 (2020).
14. Kim, J.-M. *et al.* Identification of coronavirus isolated from a patient in Korea with COVID-19. *Osong Public Health Res. Perspect.* **11**, 3–7 (2020).
15. Ivanovska, I. L. *et al.* Bacteriophage capsids: Tough nanoshells with complex elastic properties. *Proc. Natl. Acad. Sci. U. S. A.* **101**, 7600–7605 (2004).
16. Xu, X., Carrasco, C., de Pablo, P. J., Gomez-Herrero, J. & Raman, A. Unmasking imaging forces on soft biological samples in liquids when using dynamic atomic force microscopy: A case study on viral capsids. *Biophys. J.* **95**, 2520–2528 (2008).
17. Korber, B. *et al.* Spike mutation pipeline reveals the emergence of a more transmissible form of SARS-CoV-2. *bioRxiv*, 2020.2004.2029.069054 (2020).

## Acknowledgements

This study is supported by the NSF RAPID 2026657 award to MV and SS.

## Author contributions

H.S. performed the biochemical characterization A.S. performed the A.F.M. characterization, B.P., A.P. and C.E. created reagents, D.B. performed the electron microscopy characterization, M.V. and S.S. designed the research and wrote the manuscript.

## Competing interests

The authors declare no competing interests.

## Additional information

**Supplementary Information** The online version contains supplementary materials available at <https://doi.org/10.1038/s41598-020-78656-w>.

**Correspondence** and requests for materials should be addressed to M.V. or S.S.

**Reprints and permissions information** is available at [www.nature.com/reprints](http://www.nature.com/reprints).

**Publisher's note** Springer Nature remains neutral with regard to jurisdictional claims in published maps and institutional affiliations.



**Open Access** This article is licensed under a Creative Commons Attribution 4.0 International License, which permits use, sharing, adaptation, distribution and reproduction in any medium or format, as long as you give appropriate credit to the original author(s) and the source, provide a link to the Creative Commons licence, and indicate if changes were made. The images or other third party material in this article are included in the article's Creative Commons licence, unless indicated otherwise in a credit line to the material. If material is not included in the article's Creative Commons licence and your intended use is not permitted by statutory regulation or exceeds the permitted use, you will need to obtain permission directly from the copyright holder. To view a copy of this licence, visit <http://creativecommons.org/licenses/by/4.0/>.

© The Author(s) 2020